THE JOURNAL OF PHYSICAL CHEMISTRY C

Article

pubs.acs.org/JPCC

Charge Transfer Rates at a Bio−Inorganic Interface

Wenming Sun,[†] Andrea Ferretti,[†] Daniele Varsano,[†] Giorgia Brancolini,[†] Stefano Corni,[†] and Rosa Di Felice*[,†,‡]

[†]Center S3, CNR Institute of Nanoscience, Via Campi 213/A, 41125 Modena, Italy

[‡]Department of Physics and Astronomy, University of Southern California, Los Angeles, California 90089, United States

Supporting Information

ABSTRACT: We have investigated the role of molecular bridges in determining the electronic structure and transfer rates at interfaces in which natural or expanded guanine is attached through a thiol bond to a Au(111) surface as a model for charge injection at the DNA@Au interface. Our study is based on van der Waals-corrected ab initio density functional theory calculations. We have considered two linkers with different length and chemistry. We find that the shorter linker allows for a larger electronic coupling between the metal and the guanine, with a modulation of 3 orders of magnitude. The aromatic size expansion of guanine further enhances the electronic coupling by a factor of 2. Our findings demonstrate that even in the case of potentially through-bond charge transfer, the donor−acceptor distance regulates the electronic coupling. Furthermore, we establish a procedure for computing the donor−acceptor coupling between delocalized metal states and localized molecular states.

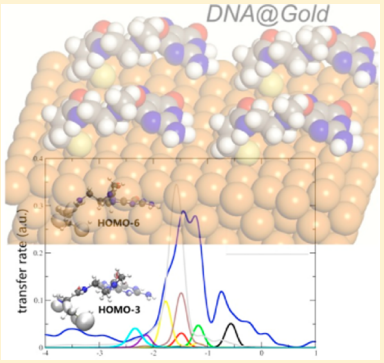

1. INTRODUCTION

Thiol functionalization of nucleic acids is a successful strategy for attaching DNA molecules to metal electrodes for electrical measurements,[1−4] biosensors,[5,6] DNA chips, and other applications.[7−9] This attachment procedure leads indeed to covalent binding,[10,11] which is needed to attain efficient charge injection into the organic part. The need for covalent molecule−electrode binding (either through thiols or other functional groups) in organic electronics has been demonstrated not only for nucleic acids but also for a variety of conductive organic molecules.[12−15]

In principle, one would like to attach thiol groups directly to the nucleic acid backbone in order to have an efficient electrical contact. However, for several years this strategy was unsuccessful for attaching DNA molecules to electrodes. Thus, alkyl chains had to be used. Scientists opted for using the smallest possible alkyl chains, namely $(CH_2)_3$,[1,2] to avoid the creation of a large electrical barrier. Yet, it is not clear to what extent this barrier affects the overall junction resistance. In more recent years, direct connection of thiols to the DNA backbone without any alkyl chain and use of such functionalized DNA molecules in break-junctions could be realized,[3] but this protocol has not yet been reproduced by other laboratories.

We undertook a theoretical study to understand the role of the linker in the charge transfer between a Au(111) substrate and a guanine base that represents the start of a DNA chain. We also considered the effect of the aromatic expansion of guanine.[16,17]

We considered interfaces formed by thiol-functionalized guanine (G) and size-expanded guanine (xG[16−19]) with the Au(111) surface. Thiol functionalization was obtained with two schemes in which both the length and chemistry of the thiol varied. Direct attachment was applied only to a neutral peptidelike backbone, specifically a poly glycine backbone terminated with a cysteine (Figure 1); we thus set up the systems Cys-GPN@Au(111) and Cys-xGPN@Au(111), where we denote 2-aminoethylglycine-carbonylmethylene-guanine as GPN and the benzene-expanded form as xGPN. Attachment to the natural Watson−Crick backbone was realized only with a spacer for G, to set up the system S-$(CH_2)_3$-DG@Au(111), where we denote guanosine as DG (Figure 1). Cys-GPN, S-$(CH_2)_3$-DG, and Cys-xGPN are in their radical form at these interfaces, which is a consensus adsorption mode for thiols on metal surfaces and the only one relevant in this study.[20−22] These systems were optimized by periodic-supercell plane-wave pseudopotential density functional theory calculations using the quantum-espresso package[23] and the vdW-DF functional.[24] The choice of the functional has been validated on base@Au(111) interfaces, and the accuracy is not limited by the revPBE exchange.[25,26]

The transfer integral, namely the electronic factor in Marcus's expression of the transfer rate,[27] is usually computed between a donor and an acceptor that are both characterized by localized orbitals. Here, a delocalized element is considered to compare through-bond and through-space efficiency in a charge-transfer reaction at a metal electrode, with metallic electron states in the formalism.

The transfer integral is a quantity that reflects the electronic coupling between a donor and an acceptor in a charge-transfer reaction.[28] It is the electronic component of the transfer

Received: July 22, 2014
Revised: July 28, 2014
Published: July 28, 2014

   dx.doi.org/10.1021/jp507346a | J. Phys. Chem. C 2014, 118, 18820−18828

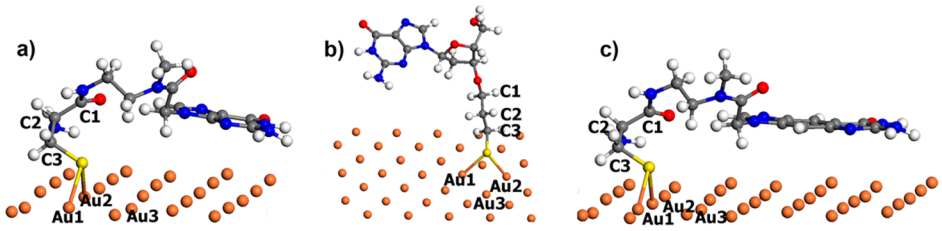

Figure 1. Optimized geometries of (a) Cys-GPN@Au(111), (b) S-$(CH_2)_3$-DG@Au(111), and (c) Cys-xGPN@Au(111) systems, in perspective view. Only the top Au layer is shown. Orange, yellow, white, gray, blue, and red spheres represent Au, S, H, C, N and O atoms, respectively. The distance between S and the two nearest-neighbor Au atoms is about 2.5 Å. The radical form of the adsorbate is obtained from the molecule by homolytic cleavage of the S−H bond.

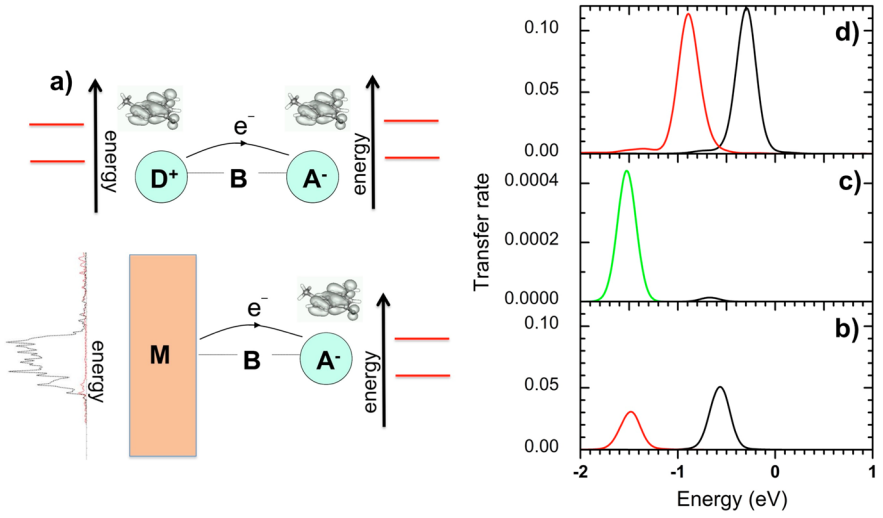

Figure 2. (a) Scheme of a donor−bridge−acceptor (D-B-A) charge-transfer reaction (top) and of a metal−bridge−acceptor (M-B-A) molecular nanojunction (bottom). The cyan circles represent molecular sites. The orange rectangle represents a metal electrode. We are interested here only at the very interface charge transfer, after which the reaction can continue through the molecular length according to the D-B-A protocol in successive steps. (b−d) Electronic transfer rate between the Au surface and the G or xG moiety as a function of the energy of the tunneling electron at the (b) Cys-GPN@Au(111), (c) S-$(CH_2)_3$-DG@Au(111), and (d) Cys-xGPN@Au(111) interface. The transfer rates are in arbitrary units, consistent with each other in b, c, and d. Contributions to the total transfer rate coming from orbitals localized on the G or xG moiety are plotted as follows: HOMO (black), HOMO−1 (red), HOMO−2 (green); this numbering conforms to the numbering of the isosurface plots in the Supporting Information and refers to the orbitals of the entire adsorbate that includes the linker (Figures S3−S5 and Table S1 in the Supporting Information). See also Figure S14 in the Supporting Information.

rate.[27,29] It is normally evaluated for molecular donor−bridge−acceptor (D-B-A) systems in which the electron (or hole) is localized in the D and A portion at the beginning and end of the reaction (Figure 2a). In reality, the situation is realized by injecting the electronic charge at a controlled location of a macromolecular complex (e.g., a DNA double helix) and revealing it at another controlled site.[30−34] In such experiments the mobile charge is supplied from discrete levels and in a finite amount. In molecular DNA nanojunctions, the DNA is attached to two extended electrodes or to an electrode and a metal-covered scanning tip;[1−3,35] in such experiments, mobile electrons and holes come from a continuous and practically infinite reservoir (the metal electrode M) under the application of a voltage and are collected at another continuous reservoir.

The computation of the transfer rate in a D-(B-)A complex is based on the determination of the molecular orbitals and their overlap. In a molecular nanojunction, one component (the electrode) is not characterized by discrete molecular levels and localized orbitals; hence, the computational procedure needs to be revised to take into account the delocalized metallic wave functions. We have done so by developing a method that is equivalent to that recently applied to an interface between molecular moieties[36] and an interface between an organic dye and an insulating substrate.[37] We find that the major aromaticity of xG relative to G and the use of a short linker enhance the donor−acceptor electronic coupling between substrate and adsorbate.

2. MATERIALS AND METHODS

A. Model Systems. The initial model for the Cys-GPN@Au(111) interface was obtained by attaching a cysteine radical through peptide bonding to a guanine extracted from a PNA strand with a poly glycine backbone (PDB entry 1XJ9).[38] The Cys-xGPN@Au(111) interface was constructed in a similar way, but with G replaced with xG, which is a size-expanded guanine derivative.[16,17] It has been shown for the special form xG4 that the introduction of a spacer conjugated ring in guanine could decrease the highest occupied molecular orbital−lowest unoccupied molecular orbital (HOMO−LUMO) gap, make the adsorption process to a gold cluster more orderly by weakening the competition between different configurations, and expand the spatial distribution of electron wave functions,[19] which makes size-expanded guanine appealing for charge-transfer performance. We expect a similar behavior for the

dx.doi.org/10.1021/jp507346a | J. Phys. Chem. C 2014, 118, 18820−18828

regular xG, based on previous results about electronic structure and transfer integrals.[18,39] The initial model for the S-$(CH_2)_3$-DG@Au(111) interface was obtained by attaching the thiol-terminated alkyl chain to guanine with its natural backbone. For the three interfaces, the bridge adsorption site was sampled, based on the stability of this S coordination detected for similar systems.[10] Namely, the S atom was accommodated above the substrate between two Au atoms of the top plane, slightly displaced toward the face-centered cubic site, and this 2-fold coordination remained stable upon full atomic relaxation. Concerning our choice of systems for comparing different linkers, we followed the following criteria: (1) include in our study the most widely used binding configuration for DNA to metal electrodes, which is the S-$(CH_2)_n$ ($n \geq 3$) linker with Watson–Crick double-stranded DNA;[1,2] (2) avoid structures that would result from hardly reproducible strategies for thiol functionalization,[3] such as the S-DG@Au(111) system; and (3) maintain the computational effort at a manageable level for producing meaningful and original results. Thus, the Cys-GPN@Au(111) interface was considered instead of S-DG@Au(111) because of the physicochemical expectation that the neutral adsorbate should bind more easily than the charged adsorbate. The alkyl linker was considered with the shortest easily reproducible chain, namely, $n = 3$. Although we ended up with linkers of different chemical nature, our results define a more general framework for interpreting the effect of the chain length; in fact, we show that the chain orbitals have little effect in the adsorbate–substrate hybridization mechanism.

B. Density Functional Theory Calculations. We carried out periodic-supercell plane-wave pseudopotential density functional theory calculations of the Cys-GPN, S-$(CH_2)_3$-DG, and Cys-xGPN radicals in contact with the Au(111) surface. We used the quantum-espresso package.[23] In order to account for van der Waals interactions, which are important at molecule@metal-surface interfaces, we adopted the vdW-DF functional.[24] This functional has given excellent results for the geometries and formation energies of a variety of similar interfaces.[25,26] The kinetic energy cutoff on the plane-wave basis set for the expansion of the electron wave functions was 25 Ry, as tested elsewhere.[26] The electron–ion interaction was described with ultrasoft pseudopotentials.[40] Valence states included the 5d and 6s shells for Au; the 2s and 2p shells for C, N and O; and the 3s and 3p shells for S. We used database pseudopotentials that were generated with the PBE functional, with scalar relativistic effects for Au. Although the functional in the atomic calculations for the generation of the pseudopotential is not fully consistent with the functional adopted in the self-consistent interface calculations, we assessed the precision of this approach on closely related systems,[25,26] and we confidently follow the same procedure here. The form of the vdW-DF functional is in principle compatible with any degree of exact exchange (hybrid functionals); for interfaces of benzene, ammonia, and cytosine with Au(111), we have found that the revPBE exchange is better than the C09 exchange for what concerns the structure and energetics, while the order of electron states is little affected.

Each interface was modeled with a periodic supercell containing a slab of Au, the adsorbed radical, and a thickness of vacuum to avoid spurious interactions between neighboring replicas. The Au slab had a lateral periodicity of $5 \times 5\sqrt{3}$, containing four layers with 50 atoms in each layer. The thickness of the vacuum layer between two slabs was 20 Å. During structure optimization, all the atoms of the substrate and adsorbate were allowed to relax until the forces vanished within 0.027 eV/Å. We employed a $(2 \times 2 \times 1)$ Monkhorst–Pack set of **k**-points for Brillouin Zone sampling.

The thiol-terminated adsorbates bind to the Au(111) surface in the radical form.[10,22] We evaluated the formation energy of each interface with respect to both the gas-phase radical (ΔE^{ads}_{rad}) and the gas-phase molecule (ΔE^{ads}_{mol}), as

$$\Delta E^{ads}_{rad} = E_{int} - E_{sur} - E_{rad} \quad (1)$$

$$\Delta E^{ads}_{mol} = 1/2E_{H_2} + E_{int} - E_{sur} - E_{mol} \quad (2)$$

In eqs 1 and 2, E_{int} is the total energy of the interface, which is composed of the substrate plus radical adsorbate; E_{sur} is the total energy of the relaxed Au(111) surface; E_{rad} is the total energy of the optimized gas-phase radical; E_{mol} is the total energy of the optimized intact adsorbate molecule, in which the thiol termination is SH; E_{H_2} is the total energy of the gas-phase H_2 molecule. The total energy calculations for the clean surface and the gas-phase molecular species were carried out in the same supercell adopted for the interface, for the sake of precision. The difference between these two interface formation energies ($\Delta E^{ads}_{rad} - \Delta E^{ads}_{mol} = E_{mol} - E_{rad} - 1/2E_{H_2}$) supplies the cleavage energy for the thiol SH bond.

C. Computation of the Electron Transfer Rate at the Molecule@Au Interface. When the system M–B–A (Figure 2a) is excited by the addition of one electron or hole, the transfer rate of electrons from M to A in a mean-field approximation can be written as

$$R^{M\to A} = \frac{1}{\hbar}\int dE[f^M(E) - f^A(E)]Tr\{\Gamma^M(E)\rho^A(E)\} \quad (3)$$

In doing so, we have considered the interface as made of two subparts, the clean Au(111) surface (M) and the gas-phase molecule (A) (Figure 2a), and then we have treated the interaction between them in a perturbative fashion, with the linker included in A. In eq 3 f^M and f^A are the occupation factors of energy levels in subsystems M and A, respectively, as a function of their orbital energy E; the trace includes the sum over spin indices; ρ^A is the spectral function (density of states) of the system A. The coupling function Γ^M can be expressed[36] in terms of Hamiltonian matrix elements as

$$\Gamma^M_{mn}(E) = 2\pi\sum_k^M V_{mk}V_{kn}\delta(E - \varepsilon^M_k) \quad (4)$$

where $V_{mk} = \langle\psi^A_m|V^{AM}|\psi^M_k\rangle$, with $\psi^{M(A)}_{k(m)}$ and $\varepsilon^{M(A)}_{k(m)}$ being the eigenstates and eigenvalues of the isolated systems M and A, and V^{AM} the interface Hamiltonian.

The advantage of this formulation is that it can be extended to treat the delocalized bands of a metal component in the coupled system. The rate $R^{M\to A}$ in eq 3 expresses the inverse lifetime of a hole created in A (say on the orbital m at energy ε^M_k) and can be recast as a Fermi golden rule, resolved by molecular orbital m:

$$R^{M\to A}_m = \frac{2\pi}{\hbar^2}\int dE\,|V_m(E)|^2\rho^M(E)\delta(E - \varepsilon^A_m) \quad (5)$$

where $V_m(E)$ is the coupling matrix element between the molecular state m and the state of the metal at energy E and the integral is over the metallic bands; $\rho^M(E)$ is the metal density of states; ε^A_m is the m eigenvalue of the molecular portion at the

dx.doi.org/10.1021/jp507346a | J. Phys. Chem. C 2014, 118, 18820–18828

Table 1. Formation Energies and Selected Structural Parameters at the Optimized Interfaces, Relative to the Isolated Substrate and Adsorbate Components

		Cys-GPN@Au(111)		S-$(CH_2)_3$-DG@Au(111)		Cys-xGPN@Au(111)	
		interface	gas phase[a]	interface	gas phase[a]	interface	gas phase[a]
interface formation energy (eV)[b]							
	ΔE_{rad}^{ads}	−2.50		−1.56		−3.72	
	ΔE_{mol}^{ads}	−1.60		−0.53		−2.29	
interface geometry[c]							
α	Au1−S−C3	107.8		108.7		111.5	
	Au2−S−C3	109.0		107.0		108.3	
	Au1−S−Au2	77.0		78.4		78.8	
	S−C3−C2	112.0	115.6	108.9	114.0	112.1	115.6
	C3−C2−C1	110.8	110.8	111.0	112.1	109.3	110.1
	C1−C2−N	110.6	110.1	107.3	107.4	111.5	114.1
d	Au1−S	2.52		2.52		2.51	
	Au2−S	2.53		2.50		2.50	
	Au3−S	3.32		3.27		3.33	
	S−C3	1.86	1.84	1.87	1.84	1.86	1.84
	Au−N	3.47				3.05	
	N−C2	1.47	1.47			1.48	1.47

[a]Gas-phase molecule. [b]Adsorption energies at the interfaces, relative to the gas-phase dehydrogenated adsorbate radical (ΔE_{rad}^{ads}) and to the gas-phase adsorbate molecule (ΔE_{mol}^{ads}), in electronvolts per radical. [c]Selected bond angles (α) and distances (d) at the interfaces and in the gas-phase molecules, in degrees and angstroms, respectively.

interface. Precisely, the curves in Figure 2b−d represent the integrand function of eq 5 for selected molecular orbitals m, after the Dirac delta term has been replaced by a finite width Gaussian centered on ε_m^A, which allows us to represent $R_m^{M\to A}$ as an energy-dependent quantity.

The transfer rate computed in this way has not exactly the same physicochemical meaning as Marcus's expression of the transfer rate between molecular centers[27] because it lacks the nuclear contribution. Yet, it expresses the same quantity, to a different level of approximation. In practice, $R_m^{M\to A}$ is the rate for the hole transfer from the molecule to the metal in absence of nuclear motions. Taking into account such motions would lead to including the thermally averaged Franck−Condon integrals in the rate calculation.[37] This contribution depends on the details of the environment surrounding A and the metal (e.g., presence of a solvent, its nature, structure of the remainder of the DNA molecule) through the reorganization energy and the redox potential. Here we want to focus instead on the intrinsic differences between the considered immobilization strategies and molecules, which are better expressed by $R_m^{M\to A}$ alone.

3. RESULTS AND DISCUSSION

A. Charge-Transfer Rates. Figure 2b−d illustrates our results on the transfer rates at the three computed interfaces.

We see in Figure 2b that at the Cys-GPN@Au(111) interface the transfer rate to and from the HOMO of guanine is dominant at small excitation energies, which are relevant to small applied voltages in a nanojunction. At larger negative energies (larger bias), the contribution of other orbitals becomes relevant to the interface transfer rate. The presence of the linker affects the values of transfer rates to HOMO and HOMO−1 to a negligible extent (Figure S14 in the Supporting Information); namely, charge transfer is mainly due to direct guanine-gold coupling.

At the S-$(CH_2)_3$-DG@Au(111) interface, we obtain a strong suppression of the transfer rate values; note the reduced rate scale in Figure 2c, as compared to that of Figure 2b. In addition, the contribution of the HOMO at small energies (small voltages) is practically negligible. The intensity of this peak decreases by a factor of about 4000 relative to Cys-GPN@Au(111); a similar factor applies if we consider the integrated HOMO peak. The presence of the linker affects the values of transfer rates to HOMO and HOMO−1 to a non-negligible extent (Figure S14 in the Supporting Information).

At the Cys-xGPN@Au(111) interface, we detect a significant enhancement of the HOMO peak relative to Cys-GPN@Au(111), by a factor of 2, whether we consider the height of the peak or the integrated area (Figure 2c). This result means that the stronger electronic coupling obtained at the interface due to the aromatic guanine expansion, which is analyzed below, will have consequences on measurable quantities. Specifically, the interface transfer rates are related to the junction resistance and therefore to measurable electrical currents.

Ultimately, we conclude from Figure 2 that the use of a short thiol chain used to attach a DNA molecule to a Au electrode in a vertical configuration should greatly enhance the interface charge transfer relative to longer chains. This rather intuitive outcome was never computed so far. The analysis of the atomic configuration, formation energy, and electronic structure of the interface corroborate this finding and allow us to interpret the reason for this behavior.

B. Atomic Structure and Stability. At the Cys-GPN@Au(111) interface (Figure 1a), the guanine heterocycle lies almost parallel to the surface, with a slight inclination. The distance between its center and the surface is 3.61 Å, which is about 0.6 Å larger than that in the case with guanine adsorbed on Au(111) without a linker.[26] The distances between the sulfur atom and the three nearest gold atoms are 2.52, 2.53, and 3.32 Å, consistent with calculations for the Cys@Au(111) system.[10] The nitrogen atom in the cysteine residue, which is not involved in peptide bonding in this short peptide, is not located on top of a gold atom as in Cys@Au(111).[21] Other geometrical parameters are collected in Table 1, together with values of the formation energy. The interface formation energy relative to the molecular adsorbate (ΔE_{mol}^{ads}) for the Cys-GPN@

dx.doi.org/10.1021/jp507346a | J. Phys. Chem. C 2014, 118, 18820−18828

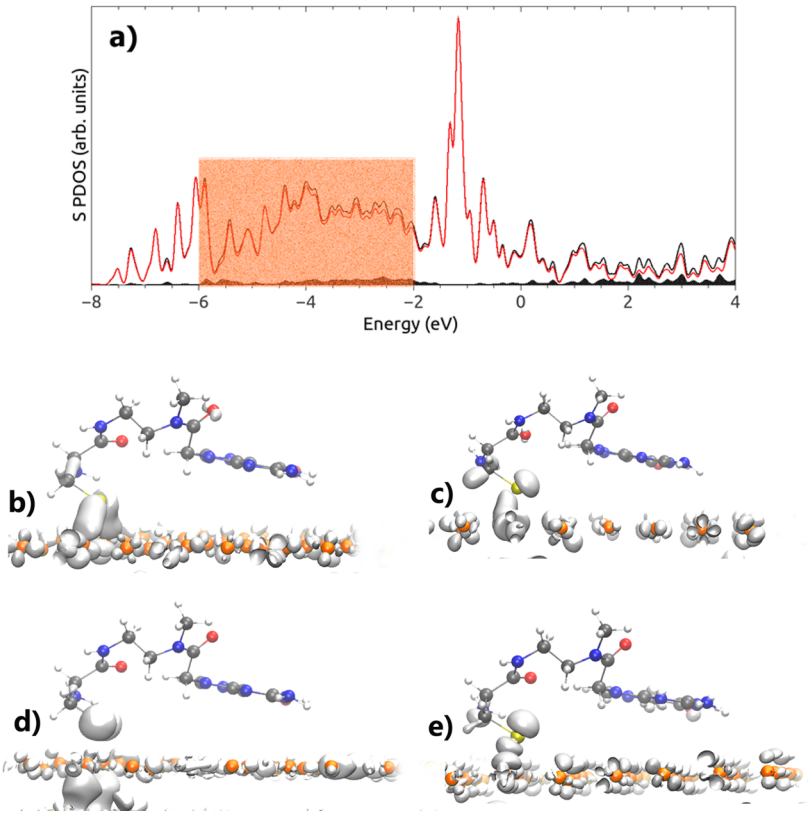

Figure 3. (a) Electronic density of states of the Cys-GPN@Au(111) interface projected on the S_s (gray area), S_p (red line) and S_{s+p} (black line) orbitals of the adsorbed radical. The shaded orange rectangle pictorially represents the extent of the Au d bands: in agreement with previous studies, the Au d orbitals (DOS not reported here) give origin to a characteristic band that extends between about 2 and 6 eV below the Fermi level.[10,41] The interface Fermi level is set at the origin of the energy scale. The presence of intense S PDOS peaks around −1 eV and between −6 and −4 eV recalls a bonding−antibonding Newns−Anderson chemisorption model typical of cysteine, which is demonstrated through the analysis of the wave functions. (b−e) Isosurface plots (isovalue = 0.0002 au) of representative bonding and antibonding orbitals resulting from S−Au hybridization at the Cys-GPN@Au(111) interface: (b) π-like bonding orbital at −4.18 eV, (c) σ-like bonding orbital at −4.17 eV, (d) π-like antibonding orbital at −0.58 eV, and (e) σ-like antibonding orbital at −0.53 eV. The energies of the illustrated orbitals are given according to the scale of Figure 3a. Orange, yellow, white, gray, blue, and red spheres represent Au, S, H, C, N, and O atoms, respectively. Similar plots for the other two computed interfaces are reported in Figures S6−S8 in the Supporting Information.

Au(111) interface is −1.60 eV, which indicates a bond formation. With the vdW-DF functional, we calculate a formation energy ΔE_{mol}^{ads} of −0.76 eV/radical for Cys@Au(111). Thus, we deduce that the G heterocycle contributes −0.84 eV/radical to the formation energy, even at the substantial distance of 3.61 Å from the surface plane.

At the S-$(CH_2)_3$-DG@Au(111) interface (Figure 1b), the guanine heterocycle is inclined relative to the surface. The linker alkyl chain is nearly perpendicular to the Au(111) plane and keeps the guanine away from the host substrate. The distance between the center of the six-membered ring in guanine and the surface is about 8.5 Å. The distances between the sulfur atom and the three nearest gold atoms are 2.52, 2.50, and 3.26 Å. The value of ΔE_{mol}^{ads} for this system is −0.53 eV, which indicates a binding sensibly weaker than that in Cys-GPN@Au(111). It is worth noting that the presence of the sugar ring is responsible for suppressing the guanine flat-lying orientation (Figure S15 in the Supporting Information).

At the Cys-xGPN@Au(111) interface (Figure 1c), the average plane of size-expanded guanine is almost parallel to the substrate, with a slight bending. The distance between the center of the spacer ring and the surface is 3.38 Å. The distance between the center of the guanine heterocycle and the surface is 3.61 Å, as in Cys-GPN@Au(111). The distances between the sulfur atom and the three nearest gold atoms are 2.51, 2.50, and 3.33 Å. The nitrogen atom in the amino group of cysteine is 3.05 Å away from its nearest gold atom, not on the top of this gold atom as in Cys-GPN@Au(111), and at odds with the Cys@Au(111) interface. The value of ΔE_{mol}^{ads} for this system is −2.29 eV, reflecting a substrate−adsorbate binding in Cys-xGPN@Au(111) that is stronger than that in Cys-GPN@Au(111). Given the similarity of the linker in the two interfaces, this difference is to be ascribed to the expanded π-conjugated aromatic ring of xG, which strongly contributes to the noncovalent binding mechanism with −1.53 eV/radical. The inclusion of van der Waals effects, which scale with molecular size, is particularly relevant to grasp such subtle features.

Summarizing the structural and energetic information, we find that the aromatic expansion of guanine yields an additional energy gain of 0.7 eV/radical when GPN and xGPN are connected to Au(111) with Cys. On the other hand, the elongation of the linker chain and the presence of the backbone in G give a weakening of the bond strength, relative to Cys-GPN@Au(111), by about 1 eV. The geometry of the radical in the adsorbed configuration remains in all cases almost identical to that of the molecule in the gas phase.

C. Electronic Structure. The plot of the total electronic density of states (DOS) projected onto the S orbitals of the

dx.doi.org/10.1021/jp507346a | J. Phys. Chem. C 2014, 118, 18820−18828

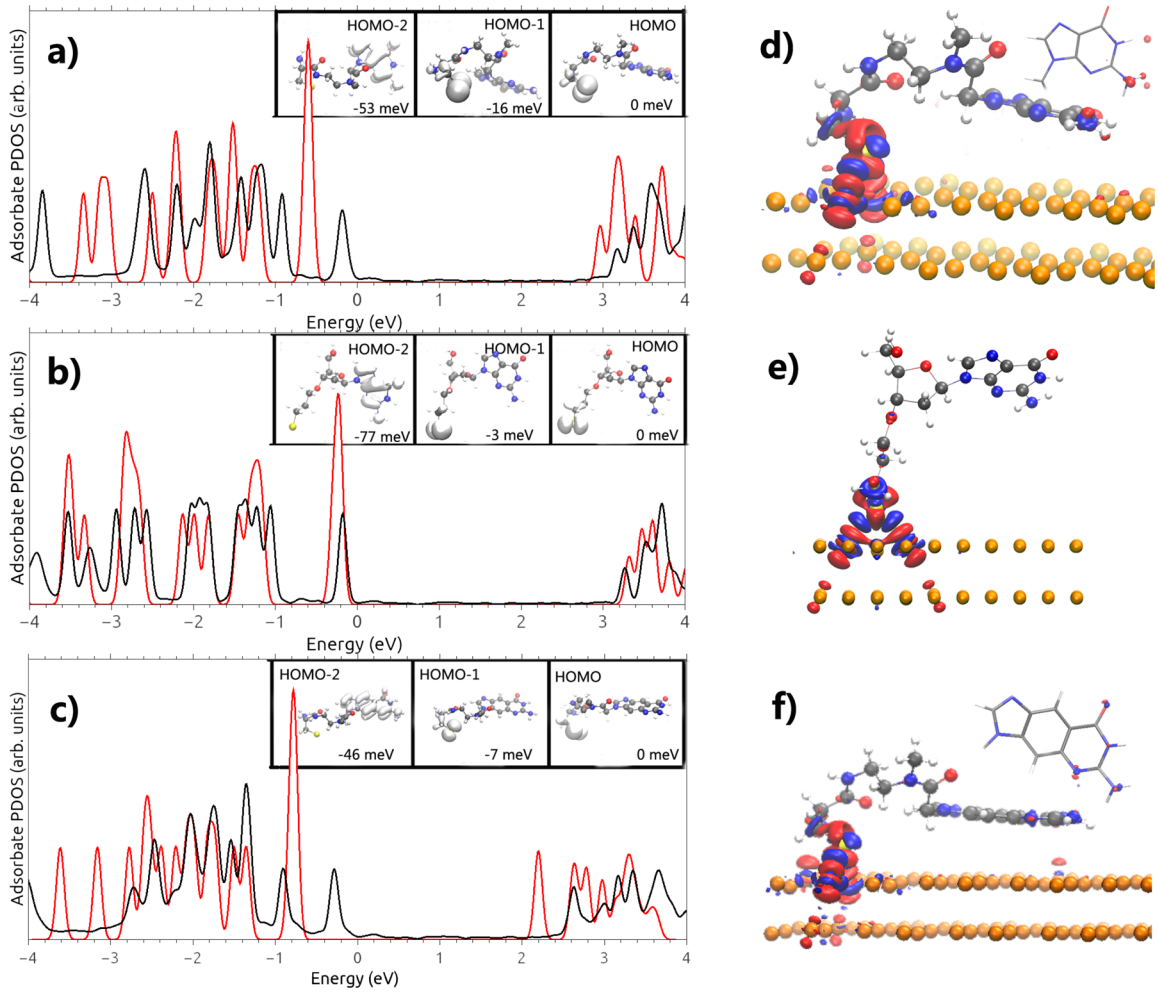

Figure 4. Left-hand side: electronic density of states of the interface projected over the molecular orbitals of adsorbate radicals (black) in (a) Cys-GPN@Au(111), (b) S-$(CH_2)_3$-DG@Au(111), and (c) Cys-xGPN@Au(111). The red line in each panel represents the total DOS of the corresponding gas-phase radical. The Fermi level is aligned with the origin of the energy scale. Isosurface plots (isovalue = 0.002 au) of frontier orbitals of the gas-phase radicals are illustrated in the insets. The energy levels in the insets of (a–c) are not aligned to each other for the different systems; the HOMO is just taken as a reference for each of them, and we wish to note the only tiny energy differences between energy levels close to the fundamental gap. Right-hand side: isosurface plots of the differential electronic density (DED) in (d) Cys-GPN@Au(111), (e) S-$(CH_2)_3$-DG@Au(111), and (f) Cys-xGPN@Au(111), with isovalue = 0.002 au. The DED is the difference between the total electron density of the interface and the electron densities of the isolated components, with the latter computed in the geometry that is the same as they have at the interface. Regions of increased electron density are indicated in blue; regions of decreased electron density are indicated in red. The insets in (d) and (f) illustrate top views of regions of electron depletion at Cys-GPN@Au(111) and Cys-xGPN@Au(111) in the G and xG moieties, respectively.

adsorbate (S PDOS) is shown in Figure 3a for the Cys-GPN@Au(111) interface.

We know that in the case of thiol-like chemisorption the S_p PDOS exhibits pronounced peaks at the upper and lower edges of the Au d band.[10] This complies with the Newns–Anderson model for atomic and molecular adsorption on metal surfaces,[41] which predicts that the interaction of a single localized orbital of the adsorbate with the narrow d band of the metal produces hybrid orbitals of both antibonding and bonding types. The single adsorbate level thus splits in two spread peaks at the edges of the metal d band: a peak with bonding character at the lower edge and a peak with antibonding character at the upper edge. This mechanism is sharp in the case of atomic adsorbates. In the case of molecular adsorbates, however, the bonding and antibonding peaks emerging from the molecule highest occupied molecular orbital are superposed to other hybrid orbitals because of intramolecule hybridization, so that especially the bonding peak is further split.[10] The PDOS(S_p) in Figure 3 (see also Figure S6 in the Supporting Information) conforms to this picture. In each of the three relaxed interfaces we find a pronounced peak in the PDOS(S_p) centered around 1 eV below the Fermi level. Inspection of the single-particle wave functions reveals the nature of this peak (Figure 3b–e). It is due to the antibonding coupling between Au d orbitals and two almost degenerate HOMOs of the radical; the latter have a p nature on S and are σ and π relative to the S–C3 bond (Figure 4a–c, insets). The corresponding S–Au (HOMO-d) bonding orbitals contribute to the several peaks between −6 and −4 eV. A similar bonding–antibonding representation is also found for S-$(CH_2)_3$-DG@Au(111) and Cys-xGPN@Au(111) (Figures S6–S8 in the Supporting Information).

From the discussion so far about the sulfur-projected DOS, we learn that the investigated systems are characterized by a strong thiol binding. However, this is not the whole story. In fact, we have seen that the base conspicuously contributes to the binding energy in the case of the short linker. Furthermore,

dx.doi.org/10.1021/jp507346a | J. Phys. Chem. C 2014, 118, 18820–18828

we know that the HOMO of guanine is very close in energy to the S_p radical HOMOs (Figure 4 and Figures S1−S5 in the Supporting Information) and contributes to intramolecule and molecule−surface hybridization. We therefore analyze in more detail the electronic density of states in search of additional features by evaluating the projections on the entire adsorbed radicals and on different portions of them. Related PDOS plots are shown in Figure 4a−c (further details are in Figures S9−S13 in the Supporting Information).

The insets in Figure 4a−c present the three highest occupied molecular orbitals for each radical. For the three H-capped molecules, the HOMO localizes on the heterocycle of G or xG and has the same charge distribution as the G and xG HOMO (Figures S1−S5 in the Supporting Information), while it shifts to the sulfur tip (S_p charge distribution) in the Cys-GPN, S-$(CH_2)_3$-DG, and Cys-xGPN radicals. Another significant feature is that the frontier orbitals in H-capped molecules are distinctly separated in energy; instead, in radicals the frontier orbitals have very similar energies. For example, the energy difference for the adjacent orbitals that localize in sulfur and heterocycles are only 37, 74, and 39 meV for Cys-GPN, S-$(CH_2)_3$-DG, and Cys-xGPN, respectively (Figure 4a−c, insets).

In Figure 4a−c, the remarkable differences between the red and black curves, which go beyond simple shifts and include changes of the shape of DOS peaks, indicate that there are strong modifications of the electronic states of the radical upon adsorption. We see here that not only the thiol orbitals are affected by these transformations. Adsorption induces the splitting of the three quasi-degenerate orbitals in the insets of Figure 4 (Figure S10 in the Supporting Information); the G or xG HOMO is shifted upward, while the thiol orbitals are shifted downward and give origin to the bonding−antibonding mixing with Au. The upward shift of the G orbital is particularly large at the Cys-GPN@Au(111) and Cys-xGPN@Au(111) interfaces, while it is quite small at the S-$(CH_2)_3$-DG@Au(111) interface. We note that the DOS changes upon adsorption for the system in Figure 4a,c involve a change of the shape, while for the system in Figure 4b there is practically a rigid shift. This is an indication of minor modification of the orbitals on guanine if the long alkyl linker is used, which is consistent with the tiny transfer rates (Figure 2).

The differential electronic density (DED) in Figure 4 is particularly revealing of the situation. Strong electron accumulation and depletion in the blue and red regions along the two S−Au bonds can be seen clearly. There is also significant electron depletion on G and xG in panels d and f of Figure 4, while there is practically no DED on G in panel e, revealing that the longer linker inhibits the participation of the G moiety in the Au−radical coupling. This is consistent with a poor efficiency of electron injection to G, which emerges from the transfer rates.

4. CONCLUSIONS

We can formulate the rationalization of the interface electron-transfer process as it unfolds from the complete analysis. When the linker chain is beyond a certain critical distance (not disclosed here), the G heterocycle does not participate in hybridization with the Au d orbitals and consequently the electronic coupling that is a component of the transfer rate is negligible. In our calculations, the two chains of different length have different chemical nature. We argue that actually the behavior is essentially due to the length. In fact, bridge orbitals and backbone orbitals do not couple significantly to Au states: thus, we expect that the electronic coupling is essentially due to the distance of the guanine from the surface. However, the presence of the thiol bond is also an important factor; (i) we know that it is efficient in stabilizing the atomic configuration of the interface, and (ii) we find that it gives modifications of the electronic density of states and (iii) modulates the orbital contribution to the transfer integral. More precisely, for a very short linker, as in Cys-GPN@Au(111), the through-space contribution dominates the charge-transfer reaction because of direct base−surface coupling. For a longer linker in which direct base−surface coupling is negligible, as in S-$(CH_2)_3$-DG@Au(111), through-bond charge transfer contributes to the interface reaction. While the relative importance of through-bond versus through-space charge transfer was previously addressed in molecular systems, we are not aware of first-principle atomistic electronic structure calculations to address this issue at a molecule−metal interface.[42]

We conceived the systems of this work as models for a Au−DNA or Au−xDNA junction where a natural or expanded guanine is the first base. Once charge is injected into G or xG through the mechanisms revealed here, it should continue into the DNA molecule according to its sequence, as proposed in many publications.[43−45] Because of the larger hybridization between Au and xG, we find that the charge injection to DNA at the Au−DNA interface with a thiol bond should be even more efficient if a modified base is used at the attachment. Joining this outcome to the fact that the electronic coupling between xGC pairs is larger than that between GC pairs,[39] we offer here striking evidence of the superior performance of aromatically expanded nucleobases for nanotechnology applications.

In conclusion, we propose the use of chemically modified bases and of the bridge chain leading to the shortest base−surface distance for thiol functionalization of DNA to optimize the electrical performance of DNA-based molecular junctions.

■ ASSOCIATED CONTENT

Ⓢ Supporting Information

Section 1, Orbitals of the Gas-Phase Molecules: illustration of isosurface plots of molecular orbitals of G, xG, Cys-GPN, HS-$(CH_2)_3$-DG, Cys-xGPN (all in saturated form) (Figures S1−S5); association of orbitals in G and xG to orbitals of the thiol-terminated Cys-GPN, HS-$(CH_2)_3$-DG and Cys-xGPN considered in this work (Table S1). Section 2, Density of States and Bonding−Antibonding Orbitals: complement of Figure 3a for the other two interfaces (Figure S6); complements of Figure 3b−e for the other two interfaces (Figures S7 and S8); illustration of the coupling of G and xG orbitals with Au electron states (Figure S9); DOS projections on different portions of the adsorbate, to illustrate that the interaction mechanism is not limited to the thiol end (Figures S10−S13). Section 3, Transfer Rates: complement of Figure 1b,c for different model interfaces in which the bridges have been cut, but the G and the substrate are constrained to the geometries of the full interfaces of Figure 1 (Figure S14). Section 4, Comment on the Geometry of S-$(CH_2)_3$-DG@Au(111): illustration of geometries of a test system S-$(CH_2)_3$-G@Au(111) (Figure S15). Section 5, References. This material is available free of charge via the Internet at http://pubs.acs.org.

■ AUTHOR INFORMATION

Corresponding Author

*E-mail: rosa.difelice@unimore.it.

Notes

The authors declare no competing financial interest.

■ ACKNOWLEDGMENTS

This work was funded by the European Commission through projects "DNA-Nanodevices" (Contract FP6-029192) and "CRONOS" (Contract FP7-280879), by the ESF through the COST Action MP0802, the Italian Institute of Technology through project MOPROSURF and the Computational Platform, Fondazione Cassa di Risparmio di Modena through Progetto Internazionalizzazione 2011, the Italian MIUR through Grant FIRB-RBFR08FOAL, and the WiSE Program at the University of Southern California. The ISCRA staff at CINECA (Bologna, Italy) is acknowledged for computational facilities and technical support. We are grateful to Marta Rosa for providing us with the value of the adsorption energy of Cys@Au(111) using quantum-espresso with the vdW-DF functional.

■ REFERENCES

(1) Cohen, H.; Nogues, C.; Naaman, R.; Porath, D. Direct Measurement of Electrical Transport Through Single DNA Molecules of Complex Sequence. *Proc. Natl. Acad. Sci. U.S.A.* **2005**, *102*, 11589−11593.

(2) Xu, B. Q.; Zhang, P. M.; Li, X. L.; Tao, N. J. Direct Conductance Measurement of Single DNA Molecules in Aqueous Solution. *Nano Lett.* **2004**, *4*, 1105−1108.

(3) Kang, N.; Erbe, A.; Scheer, E. Electrical Characterization of DNA in Mechanically Controlled Break-Junctions. *New J. Phys.* **2008**, *10*, 023030.

(4) Slinker, J. D.; Muren, N. B.; Renfrew, S. E.; Barton, J. K. DNA Charge Transport Over 34 nm. *Nat. Chem.* **2011**, *3*, 228−233.

(5) Furst, A. L.; Hill, M. G.; Barton, J. K. DNA-Modified Electrodes Fabricated Using Copper-Free Click Chemistry for Enhanced Protein Detection. *Langmuir* **2013**, *29*, 16141−16149.

(6) Drummond, T. G.; Hill, M. G.; Barton, J. K. Electrochemical DNA Sensors. *Nat. Biotechnol.* **2003**, *21*, 1192−1199.

(7) Steel, A. B.; Levicky, R. L.; Herne, T. M.; Tarlov, M. J. Immobilization of Nucleic Acids at Solid Surfaces: Effect of Oligonucleotide Length on Layer Assembly. *Biophys. J.* **2000**, *79*, 975−981.

(8) Niemeyer, C. M. Nanoparticles, Proteins, and Nucleic Acids: Biotechnology Meets Materials Science. *Angew. Chem., Int. Ed.* **2001**, *40*, 4128−4158.

(9) Sokolova, V.; Epple, M. Inorganic Nanoparticles As Carriers of Nucleic Acids Into Cells. *Angew. Chem., Int. Ed.* **2008**, *47*, 1382−1395.

(10) Di Felice, R.; Selloni, A.; Molinari, E. DFT Study of Cysteine Adsorption on Au(111). *J. Phys. Chem. B* **2003**, *107*, 1151−1156.

(11) Hakkinen, H. The Gold−Sulfur Interface at the Nanoscale. *Nat. Chem.* **2012**, *4*, 443−455.

(12) Venkataraman, L.; Klare, J. E.; Tam, I. W.; Nuckolls, C.; Hybertsen, M. S.; Steigerwald, M. L. Single-Molecule Circuits with Well-Defined Molecular Conductance. *Nano Lett.* **2006**, *6*, 458−462.

(13) Kim, B.; Choi, S. H.; Zhu, X. Y.; Frisbie, C. D. Molecular Tunnel Junctions Based on π-Conjugated Oligoacene Thiols and Dithiols between Ag, Au, and Pt Contacts: Effect of Surface Linking Group and Metal Work Function. *J. Am. Chem. Soc.* **2011**, *133*, 19864−19877.

(14) Frei, M.; Aradhya, S. V.; Hybertsen, M. S.; Venkataraman, L. Linker Dependent Bond Rupture Force Measurements in Single-Molecule Junctions. *J. Am. Chem. Soc.* **2012**, *134*, 4003−4006.

(15) Quek, S. Y.; Venkataraman, L.; Choi, H. J.; Louie, S. G.; Hybertsen, M. S.; Neaton, J. B. Amine-Gold Linked Single-Molecule Circuits: Experiment and Theory. *Nano Lett.* **2007**, *7*, 3477−3482.

(16) Gao, J.; Liu, H.; Kool, E. T. Assembly of the Complete Eight-Base Artificial Genetic Helix, xDNA, and Its Interaction with the Natural Genetic System. *Angew. Chem., Int. Ed.* **2005**, *44*, 3118−3122.

(17) Liu, H.; Gao, J.; Kool, E. T. Size-Expanded Analogues of dG and dC: Synthesis and Pairing Properties in DNA. *J. Org. Chem.* **2005**, *70*, 639−647.

(18) Varsano, D.; Garbesi, A.; Di Felice, R. Ab Initio Optical Absorption Spectra of Size-Expanded xDNA Base Assemblies. *J. Phys. Chem. B* **2007**, *111*, 14012−14021.

(19) Sun, W.; Di Felice, R. Nature of the Interaction between Natural and Size Expanded Guanine with Gold Clusters: A Density Functional Theory Study. *J. Phys. Chem. C* **2012**, *116*, 24954−24961.

(20) Gronbeck, H.; Curioni, A.; Andreoni, W. Thiols and Disulfides on the Au(111) Surface: The Headgroup-Gold Interaction. *J. Am. Chem. Soc.* **2000**, *122*, 3839−3842.

(21) Di Felice, R.; Selloni, A. Adsorption Modes of Cysteine on Au(111): Thiolate, Amino-Thiolate, Disulfide. *J. Chem. Phys.* **2004**, *120*, 4906−4914.

(22) Vargas, M. C.; Giannozzi, P.; Selloni, A.; Scoles, G. Coverage-Dependent Adsorption of CH_3S and $(CH_3S)_2$ on Au(111): A Density Functional Theory Study. *J. Phys. Chem. B* **2001**, *105*, 9509−9513.

(23) Giannozzi, P.; Baroni, S.; Bonini, N.; Calandra, M.; Car, R.; Cavazzoni, C.; Ceresoli, D.; Chiarotti, G. L.; Cococcioni, M.; Dabo, I.; et al. QUANTUM ESPRESSO: A Modular and Open-Source Software Project for Quantum Simulations of Materials. *J. Phys.: Condens. Matter* **2009**, *21*, 395502.

(24) Dion, M.; Rydberg, H.; Schroder, E.; Langreth, D. C.; Lundqvist, B. I. Van der Waals Density Functional for General Geometries. *Phys. Rev. Lett.* **2004**, *92*, 246401.

(25) Rosa, M.; Corni, S.; Di Felice, R. A Density Functional Theory Study of Cytosine on Au(111). *J. Phys. Chem. C* **2012**, *116*, 21366−21373.

(26) Rosa, M.; Corni, S.; Di Felice, R. Interaction of Nucleic Acid Bases with the Au(111) Surface. *J. Chem. Theory Comput.* **2013**, *9*, 4552−4561.

(27) Marcus, R. A.; Sutin, N. Electron Transfers in Chemistry and Biology. *Biochim. Biophys. Acta* **1985**, *811*, 265−322.

(28) Migliore, A. Full-Electron Calculation of Effective Electronic Couplings and Excitation Energies of Charge Transfer States: Application to Hole Transfer in DNA π-Stacks. *J. Chem. Phys.* **2009**, *131*, 114113.

(29) Warshel, A.; Parson, W. W. Computer-Simulations of Electron-Transfer Reactions in Solution and in Photosynthetic Reaction Centers. *Annu. Rev. Phys. Chem.* **1991**, *42*, 279−309.

(30) Kelley, S. O.; Barton, J. K. Electron Transfer Between Bases in Double Helical DNA. *Science* **1999**, *283*, 375−381.

(31) Murphy, C. J.; Arkin, M. R.; Jenkins, Y.; Ghatlia, N. D.; Bossmann, S. H.; Turro, N. J.; Barton, J. K. Long-Range Photoinduced Electron-Transfer Through a DNA Helix. *Science* **1993**, *262*, 1025−1029.

(32) Giese, B.; Amaudrut, J.; Kohler, A. K.; Spormann, M.; Wessely, S. Direct Observation of Hole Transfer through DNA by Hopping Between Adenine Bases and by Tunnelling. *Nature (London, U.K.)* **2001**, *412*, 318−320.

(33) Schwogler, A.; Burgdorf, L. T.; Carell, T. Self-Repairing DNA Based on a Reductive Electron Transfer through the Base Stack. *Angew. Chem., Int. Ed.* **2000**, *39*, 3918−3920.

(34) Henderson, P. T.; Jones, D.; Hampikian, G.; Kan, Y. Z.; Schuster, G. B. Long-Distance Charge Transport in Duplex DNA: The Phonon-Assisted Polaron-Like Hopping Mechanism. *Proc. Natl. Acad. Sci. U.S.A.* **1999**, *96*, 8353−8358.

(35) Porath, D.; Bezryadin, A.; de Vries, S.; Dekker, C. Direct Measurement of Electrical Transport through DNA Molecules. *Nature (London, U.K.)* **2000**, *403*, 635−638.

(36) Schiros, T.; Kladnik, G.; Prezzi, D.; Ferretti, A.; Olivieri, G.; Cossaro, A.; Floreano, L.; Verdini, A.; Schenck, C.; Cox, M.; et al. Donor−Acceptor Shape Matching Drives Performance in Photovoltaics. *Adv. Energy Mater.* **2013**, *3*, 894−902.

(37) Maggio, E.; Martsinovich, N.; Troisi, A. Evaluating Charge Recombination Rate in Dye-Sensitized Solar Cells from Electronic Structure Calculations. *J. Phys. Chem. C* **2012**, *116*, 7638−7649.

(38) Petersson, B.; Nielsen, B. B.; Rasmussen, H.; Larsen, I. K.; Gajhede, M.; Nielsen, P. E.; Kastrup, J. S. Crystal Structure of a Partly Self-Complementary Peptide Nucleic Acid (PNA) Oligomer Showing a Duplex-Triplex Network. *J. Am. Chem. Soc.* **2005**, *127*, 1424−30.
(39) Migliore, A.; Corni, S.; Varsano, D.; Klein, M. L.; Di Felice, R. First Principles Effective Electronic Couplings for Hole Transfer in Natural and Size-Expanded DNA. *J. Phys. Chem. B* **2009**, *113*, 9402−9415.
(40) Vanderbilt, D. Soft Self-Consistent Pseudopotentials in a Generalized Eigenvalue Formalism. *Phys. Rev. B: Condens. Matter Mater. Phys.* **1990**, *41*, 7892−7895.
(41) Hammer, B.; Norskov, J. K. Theory of Adsorption and Surface Reactions. *NATO ASI, Ser. E* **1997**, *331*, 285−351.
(42) Kurlancheek, W.; Cave, R. J. Tunneling through Weak Interactions: Comparison of Through-Space-, H-Bond-, and Through-Bond-Mediated Tunneling. *J. Phys. Chem. A* **2006**, *110*, 14018−14028.
(43) *Charge Transfer in DNA: From Mechanism to Application*; Wagenknecht, H.-A., Ed.; Wiley: Hoboken, NJ, 2005.
(44) *Long-Range Charge Transfer Through DNA I*; Schuster, G. B., Ed.; Springer: Berlin, 2004.
(45) *Long-Range Charge Transfer Through DNA II*; Schuster, G. B., Ed.; Springer: Berlin, 2004.